OGT Controls the Expression and the Glycosylation of E-cadherin, and Affects Glycosphingolipid Structures in Human Colon Cell Lines

James Biwi, Charlotte Clarisse, Christophe Biot, Radoslaw Pawel Kozak, Katarina Madunic, Marlène Mortuaire, Manfred Wuhrer, Daniel Ian Richard Spencer, Céline Schulz, Yann Guérardel, et al.

OGT controls the expression and the glycosylation of E-cadherin, and affects glycosphingolipid structures in human colon cell lines

James Biwi[1], Charlotte Clarisse[1], Christophe Biot[1], Radoslaw P. Kozak[2], Katarina Madunic[3], Marlène Mortuaire[1,] Manfred Wuhrer[3], Daniel I.R. Spencer[2], Céline Schulz[1], Yann Guerardel[1], Tony Lefebvre[1]*, and Anne-Sophie Vercoutter-Edouart[1]

[1]Université de Lille, CNRS, UMR 8576, UGSF, Unité de Glycobiologie Structurale et Fonctionnelle, F-59000, Lille, France.
[2]Ludger Ltd, Culham Science Centre, Abingdon, Oxfordshire, United Kingdom.
[3]Leiden University Medical Centre, Centre for Proteomics and Metabolomics, Leiden, Netherlands.

* Corresponding author: tony.lefebvre@univ-lille.fr

Abstract

Colorectal cancer (CRC) affects both women and men living in societies with a high sedentary lifestyle. Amongst the phenotypic changes exhibited by tumor cells, a wide range of glycosylations has been reported for colon cancer-derived cell lines and CRC tissues. These aberrant modifications affect different aspects of glycosylation, including an increase in core fucosylation and GlcNAc branching on *N*-glycans, alteration of *O*-glycans, upregulated sialylation and *O*-GlcNAcylation. Although *O*-GlcNAcylation and complex glycosylations differ in many aspects, sparse evidences report on the interference of *O*-GlcNAcylation with complex glycosylation. Nevertheless, this relationship is still a matter of debate. Combining different approaches on three human colon cell lines (HT29, HCT116 and CCD841CoN), we herein report that silencing *O*-GlcNAc transferase (OGT, the sole enzyme driving *O*-GlcNAcylation), only slightly affects overall *N*- and *O*-glycosylation patterns. Interestingly, silencing of OGT in HT29 cells upregulates E-cadherin (a major actor of epithelial-to-mesenchymal transition) and changes its glycosylation. On the other hand, OGT silencing perturbs biosynthesis of glycosphingolipids resulting in a decrease in gangliosides and an increase in globosides. Together, these results provide novel insights regarding the selective regulation of complex glycosylations by *O*-GlcNAcylation in colon cancer cells.

Abbreviations: CRC, colorectal cancer; GH, glycosylhydrolase; GSL, glycosphingolipids; GT, glycosyltransferase; HBP, hexosamine biosynthetic pathway; OGT, *O*-GlcNAc transferase

Keywords: colon cancer, E-cadherin, glycomics, glycosphingolipids, *O*-GlcNAcylation

1. Introduction

Glycans are a large family of post-translational modifications (PTM) made from a single or combinations of monosaccharides that play key-roles at each level of cellular homeostasis. Glycosylations may be simple from a structural point of view, as is the case with *O*-GlcNAcylation confined within the nucleocytoplasmic and mitochondrial compartments, or much more complex such as mucin-type *O*-Glycans, *N*-glycans and glycosaminoglycans [1-2]. Apart from proteins, glycans modify other types of molecules such as lipids – glycosphingolipids (GSL) or glycosylphosphatidylinositols – generating highly complex structures [3].

Alteration of glycosylation is one of the hallmarks of cancer cells. These abnormalities are the consequence of altered expression of genes encoding GTs (glycosyltransferases) and GHs (glycosylhydrolases), nucleotide-sugar transporters and any other protein involved in glycosylation. Variabilities in nucleotide-sugar supply or defects in the intracellular trafficking machinery may also contribute to tumorigenesis. Consequently, and specifically in colorectal cancer (CRC), these perturbations lead to abnormal glycosylation profiles including branched and sialylated *N*-glycans, truncated mucin-type *O*-glycans, increased fucosylation and sialylation of Lewis antigens and aberrant *O*-GlcNAcylation [4-5]. Numerous studies have reported an increased level of *O*-GlcNAcylation in cancers with the consequence of aberrant stabilization of oncogenic factors [6], sustained proliferation, increased migration, invasion, and metastasis [7-9]. Conversely, very few studies investigated the putative regulation of complex glycosylations by *O*-GlcNAcylation. Phoomak *et al*. recently demonstrated in cholangiocarcinoma that *O*-GlcNAc transferase (OGT), the enzyme catalyzing *O*-GlcNAcylation process, positively controls the degradation of the transcription factor FOXO3 through the activation of PI3K and MAPK pathways [10]. Consequently, the Golgi mannosidase MAN1A1, a target gene of FOXO3 which drives high-mannose structures trimming, is downregulated. Throughout this study, the authors highlighted how *O*-GlcNAcylation affects cancer cells surface *N*-glycosylation. On the other hand, OGT binds and controls many transcriptional regulators including TET proteins [11]. Silencing of OGT in mouse embryonic stem cells led to up- or down-regulation of several genes involved in *N*- and *O*-glycosylation processes [11].

The end-product of hexosamine biosynthetic pathway (HBP) is the nucleotide sugar UDP-GlcNAc, which is used by all GlcNAc transferases including OGT. UDP-GlcNAc can be converted into UDP-GalNAc and CMP-NeuAc [5,12]. The originator study on *C. elegans* showed that silencing *ogt* gene modifies UDP-HexNAc and UDP-Glc levels, which may affect general glycosylation patterns [13]. Similar effect is observed after silencing *oga,* the gene that encodes the *O*-GlcNAcase removing *O*-GlcNAc residues (OGA). In *ogt-ko* worms, mRNA levels of gfat (glutamine:fructose-6-phosphate amidotransferase)-2 and gna (glucosamine-6-phosphate N-acetyltransferase)-2, two enzymes of the

HBP and a putative UDP-GlcNAc pyrophosphorylase are more elevated [13]. In human colon cancer GFAT is overexpressed and its silencing provoked cell surface glycosylation modifications [12]. Therefore, interfering with HBP should induce defects in multiple glycosylation processes, as most glycans require UDP-GlcNAc for at least one step of their biosynthesis [14-15].

Previously, we established that silencing OGT (siOGT) impairs formation of colonies, migration, proliferation and adhesion abilities of CRC cell lines HT29 and HCT116 and the fetal colon cell line CCD841CoN [9]. Growing knowledge shows that complex glycans are important for the above cell properties [2]. We then set forth to establish the impact of siOGT on complex glycosylation in HT29, HCT116 and CCD841CoN cells. By combining glycomics, transcriptomics, and several cellular approaches, we show that silencing OGT in human colon cell lines does not strongly affect the *N*- and *O*-glycan structures, albeit mRNA levels of several GTs and GHs were downregulated. On the other hand, OGT silencing in HT29 cells upregulates E-cadherin, an integral protein necessary for cell adhesion, and affects its glycosylation. Lastly, we point out variations of GSLs synthesis following OGT-silencing, characterized by a global increase in globosides and decrease in gangliosides levels. Altogether our data indicates that the nucleocytoplasmic *O*-GlcNAc modification partly drives complex glycosylations in colon cell lines and that the differences observed are cell line-dependent.

2. Materials and methods

2.1 Antibodies and Lectins

Antibodies and lectins used in this study are summarized in supplementary data.

2.2 Cell culture and small interfering RNA reverse transfection

Human fetal colon CCD841CoN, colon adenocarcinoma HT29 and colon carcinoma HCT116 cells were grown as previously described [9]. Small interfering RNA (siRNA) reverse transfection were performed using siRNA Control (siRNA universal negative control 1, Sigma) or siOGT (GGA GGC UAU UCG AAUCAG U[dT][dT] forward, ACU GAU UCG AAU AGC CUCC[dT][dT] reverse, Sigma) [9]. Cells were harvested 72 hours after transfection.

2.3 Transcriptomics

SiRNA-transfected cell monolayers were washed twice in ice-cold PBS and harvested. After centrifugation, cell pellets (10^6 cells) were frozen at -80°C and further processed by Qiagen for transcriptomic analysis (Qiagen, Hilden, Germany). The p-values were calculated based on a

Student's t-test of the replicate 2^(-DeltaCt) values for each gene in the siControl and siOGT groups (3 biological replicates per group) (two-tailed distribution, two-sample unpaired).

2.4 Immunoprecipitation and Western blotting

siRNA-transfected HT29 cells were lysed in lysis buffer (50 mM Tris pH 7.5, 150 mM NaCl, 1% NP-40, 0.25% sodium deoxycholate and 0.1% SDS and protease inhibitors). Immunoprecipitation and Western blotting were performed as previously described [16], except for the detection of Sd^a antigen which was revealed with a specific antibody as described by Groux *et al*. [17]. Lectin blotting was performed as described in the supplemental file. Quantification of ECL or fluorescent signal was measured by densitometry using the ImageJ® software. Student's *t*-test was used for statistical analysis; *p*-values were calculated and reported accordingly.

2.5 Lectin labeling and flow cytometry analysis

Cell monolayer was washed twice in PBS, harvested using 5 mM EDTA in PBS and placed in a microtube. After centrifugation (400 x *g*, 5min), cells were incubated with labeled lectins (suppl. file) in 50 µl PBS containing 1% BSA for 1 h at 4 °C. After incubation with biotin-conjugated lectins, cells were washed once in PBS, centrifuged, and then incubated with DyLight 488 Streptavidin in PBS-1% BSA for 1 h at 4 °C. Then cells were washed three times in PBS before FACS analysis. For labeling with FITC-labeled lectins, cells were directly washed three times in PBS. Fluorescence was measured in the FL1 channel using a FACSCalibur cytometer (Becton Dickinson). Quantification of flow cytometry analysis was done by using FlowJo software (vX 0.7).

2.6 Indirect Immunofluorescence and confocal microscopy

Cells were transfected with siRNA (si Control, siOGT) and grown in 6-well plates on glass coverslips for 3 days. Cells were fixed as previously described and directly incubated with E-cadherin primary antibody and lectin, followed by incubation with secondary antibody and DyLight 488 Streptavidin [16]. Images were acquired using an inverted Zeiss LSM700 confocal microscope with a 40x oil immersion lens and data were collected with the ZEN 2010 software (Zeiss). Images were processed with ImageJ® and quantification was done using a homemade plugin developed by TISBio to detect and quantify the fluorescence in cells. Scatter dot plot (median with interquartile range) showing fluorescence intensity quantified in each cell (two captured images per condition) and statistical analysis were obtained using GraphPad Prism software (Student's *t*-test, ***, $p<0.0001$).

2.7 Cell harvest for MS

Following transfections, cells were retrieved on ice and washed 3 times with PBS, harvested using 5 mM EDTA with incubation at 37 °C, then retrieved into 15 mL tubes using PBS and centrifuged (650 x *g*, 5 min). Cells were washed twice in PBS and resuspended in 10 mL PBS before counting. Finally, cells were aliquoted into $3x10^6$ (for *N*-glycomics) or $2x10^6$ (for *O*-glycomics and GSL analysis) cells per microtube, centrifuged (13.800 x *g*, 15 min) and the pellets were stored at - 20 °C until further use.

2.8 *N*-glycan release from cell lysates and MS analysis

N-glycans were released from glycoproteins of cell pellets ($3x10^6$ cells) of two biological replicates, using LudgerZyme™ PNGase F Release Kit (Ludger Ltd). Briefly, samples were homogenized for 45 minutes in a sonication bath followed by centrifugation (500 x g, 15 min). Nine µL of pure water and 1 µL of denaturing buffer were added to each sample and mixed. Samples were incubated at 100°C for 10 min to denature the proteins. After cooling the samples to RT, 2 µL of 10X reaction buffer, 2 µL of 10% NP-40 solution, 6 µL of pure water and 1 µL of PNGase F were added to each sample. Samples were vortexed and then incubated overnight at 37°C. The released glycans were then converted to aldoses with 0.1% formic acid, filtered through a protein-binding membrane and dried [18]. Released *N*-glycans were fluorescently labelled by reductive amination with procainamide using LudgerTag™ Procainamide Glycan Labelling Kit (LT-KPROC-24) as described previously [19].
Procainamide-labelled *N*-glycan samples and system suitability standards were analysed by HILIC-(U)HPLC-ESI-MS with fluorescence detection, using the previously described protocol [18]. Relative glycan quantification was achieved using HappyTools software, allowing automated peak, background and noise detection [20]. Relative abundance of each identified labelled *N*-glycan peak was calculated as a percentage of the total AUC of peaks detected ($\%x = [AUC_x/\sum(AUC)_n] \times 100\ \%$) in the time range 10-45 min.

2.9 *O*-Glycan Release and MS analysis

The previously reported protocol by Jensen *et al.* was used to sequentially release *N*-glycans and *O*-glycans from the single pools of glycoproteins [21]. Approximately $0.5x10^6$ cells per sample from 4 biological replicates were used for the release of *O*-glycans. Briefly, samples were blotted on PVDF membrane, *N*-glycans were released using 2 U PNGase F enzyme (Roche) by incubation overnight at 37 °C, as previously reported [22]. *O*-Glycan release, reduction, desalting and purification steps were performed as described in [21] (see Suppl. file). *O*-glycan analysis was performed using a nano-porous graphitized carbon liquid chromatography Ultimate 3000 UHPLC system (Dionex/Thermo Fisher Scientific) coupled to an amaZon ETD speed ion trap (Bruker, Bremen, Germany) (PGC-LC-MS/MS). Details are included in the supplementary file. Assignment of monosaccharide composition from identified glycan masses (m/z) was aided by searching in GlycoMod portal

(www.expasy.org/glycomod/). Relative glycan abundance was calculated from the area under the extracted ion chromatogram (EIC) area peak of the parent m/z ion as a percentage of the total EIC peak areas. All glycan structures were drawn and theoretical mass assigned using GlycoWorkbench (Version 2.1, www.eurocarbdb.org/).

2.10 Glycosphingolipid analysis by MS

Approximately $2x10^6$ cells per sample from 3 biological replicates were used to isolate and permethylate GSLs, before QIT-TOF-MALDI analysis. Cells were lyophilized, extracted twice with $CHCl_3/CH_3OH$ (2:1, v/v), twice with $CHCl_3/CH_3OH$ (1:2, v/v) and finally $CHCl_3/CH_3OH/H_2O$ (1:2:0.8). Combined supernatants were dried under a nitrogen stream, subjected to mild saponification with 0.1 M NaOH in $CHCl_3/CH_3OH$ (1:1, v/v) at 37 °C for 2 h, and evaporated to dryness. Samples were resuspended in CH_3OH/0.1% TFA in water (1:1, v/v) and applied to reverse-phase C18 cartridges (200 mg, Interchim, France). Columns were pre-activated using $CHCl_3/CH_3OH$ (2:1), CH_3OH and finally CH_3OH/0.1 % TFA in water (1:1). Then samples were loaded on to the column, columns were washed with CH_3OH/0.1 % TFA in water and finally glycolipids were eluted sequentially with CH_3OH (1 column volume), followed by 2 column volumes of $CHCl_3/CH_3OH$ (2:1). Eluted glycolipids were dried and subjected to permethylation. Permethylation was carried out using the Ciucana and Kerek method [23]. Briefly, the compounds were resuspended in DMSO/NaOH/ICH_3 and agitated for 2 h. The derivatisation was stopped by dropwise addition of cold water and permethylated GSLs were extracted in $CHCl_3$ and washed at least 7 times in water. Per-methylated GSLs were resuspended in 100 µL of chloroform/methanol (1:2, v/v). 0.5 µL sample was mixed with 0.5 µL of DHB matrix solution (10 mg/mL in chloroform/methanol 2:1, *v/v*) and spotted on MALDI plate. MALDI-QIT spectra were acquired on MALDI-QIT-TOF Shimadzu AXIMA Resonance mass spectrometer in positive mode. The mid mode (mass range m/z 1000-3000) was used with laser power set at 85 for 2 shots in 100 locations per spot. Assignment was made tentatively from calculated mass composition and a literature search [24, 25].

3. Results

3.1 Global GTs and GHs transcriptomic analysis in OGT-silenced colon cell lines

We first sought to decipher the influence of OGT silencing on the mRNA levels of various GTs and GHs in the colon cancer cell lines HT29 and HCT116, and the non-cancerous and control CCD841CoN cell line. Cells were silenced of OGT by siRNA or transfected with siControl for 72 h. OGT silencing was confirmed by transcriptomic analysis (Fig. S1): OGT mRNA levels decreased by 10-fold in CCD841CoN, by 4-fold in HT29 and by 13-fold in HCT116 cells. Down-regulation at the protein level

was elucidated by Western-blot against OGT and *O*-GlcNAcylated proteins (Fig. S1C). The specificity of the anti-*O*-GlcNAc antibody was checked by incubation with excess of free GlcNAc (Fig. S1D). In the three cell lines, silencing of OGT was found to be accompanied by a corresponding decrease in OGA mRNA and protein expression as previously reported [1].

The mRNA profiles of 86 GTs and GHs involved in the synthesis of a wide range of glycans were compared between the two conditions (Table S1). Several genes were upregulated or downregulated in siOGT cells but only a change of at least twofold with a p-value <0.05 was considered significant in this study (Fig. S1). siOGT HT29 cells did not show any significant changes in any GTs and GHs mRNA levels. However, in siOGT HCT116 cells we observed a downregulation of the following genes: MANBA (lysosomal *N*-glycan catabolism), ST8SIA6 (*O*-Glycans, core 1 disialylation), GALNT8 (*O*-Glycans) and core 2 synthase GCNT3 (*O*-Glycans, mucin-type). Similarly, siOGT CCD841CoN cells exhibited downregulation of genes namely, FUT8 (*N*-glycan, core fucosylation), MGAT5B (Branching *N*- and *O*-Mannose glycans), and the two mucin-type *O*-Glycan synthesis initiators GALNT6 and GALNT16 (Fig. S1). This first experiment shows that silencing OGT downregulates mRNA levels of very few GTs and GHs in a cell type-dependent manner.

3.2 Global survey of cell surface glycosylation in OGT-silenced colon cell lines

To establish whether OGT silencing affects cell surface glycome of colon cells, we used lectins that target *O*-glycans (jacalin), β1,6-branching *N*-glycans (L-PHA), terminal sialylation (MAA for α2,3 and SNA for α2,6) and fucosylation (AAA for α1,6-fucosylation and α1,2/α1,3/4-fucosylation with UEA). By flow cytometry, we assayed the binding of each lectin at the cell surface and compared the fluorescent labeling between siControl and siOGT conditions (Fig. 1). L-PHA labeling increased slightly in siOGT CRC cells, whereas no significant change was observed in CCD841CoN cells. Regarding fucosylation, cell surface labeling with AAA was reduced only in siOGT-HT29 cells, while UEA labeling declined in siOGT-CCD841CoN cells. Jacalin binding did not change except in HCT116 cells where it tended to increase upon silencing of OGT. Finally, these experiments showed that α2,3-sialylation but not α2,6-sialylation, was sensitive to siOGT in the three cell lines: while MAA labeling decreased in siOGT CCD841CoN cells, it slightly increased in the CRC cell lines HT29 and HCT116 (Fig. 1). Given the strong decrease of α2,3-sialylation in siOGT-CCD841CoN cells, we further investigated whether the Sd^a antigen (GalNAcβ1-4[Neu5Acα2-3]Galβ) could be downregulated in these cells. Detection of Sd^a by Western-blot using a specific antibody shows a 20-30% decrease on glycoproteins from siOGT-CCD841CoN cells (Fig. S2). As previously shown, no Sd^a was detected in the two CRC cell lines HT29 and HCT116 [17]. This set of experiments indicates that disturbance in α2,6-sialylation is not

significant in siOGT cells while α2,3-sialylation increases in the two colon cancer cell lines and decreases in the non-cancerous colon cell line.

3.3 Global *N*-Glycomic survey in OGT-silenced colon cells

We then investigated the effect of siOGT transfection on *N*-glycan profile in the three cell lines. The global *N*-glycan traits were elucidated by HILIC-(U)HPLC-ESI-MS analysis of procainamide-labelled glycans (Fig. 2A). Structures were assigned using MS/MS fragments (Table S2). While similarities are found between the colon cell lines' *N*-glycan profiles, many differences were also observed. In particular, HT29 cells exhibited a very simple *N*-glycan profile dominated by oligomannosylated structures whereas CCD841CoN cells showed a high diversity of complex *N*-glycans including bisecting GlcNAc-containing structures (elution time at 23.2, 25.0 and 26.2 mins) and Sd^a-containing structures (29.1 min) (Fig. 2B), both known to be downregulated in cancer cells [4,17].

No major differences between siOGT- versus siCtrl-transfected cells were noted except for some slight modifications in the respective proportions of *N*-glycans (Fig. 2B). In HCT116 cells, the high mannose structures MAN7 ($Hex_7HexNAc_2$, 27.1 min) and MAN8 ($Hex_8HexNAc_2$, 30.0 min), showed a 1.20 and 1.30-fold increase respectively. Similarly, for CCD841CoN cells a 1.40-fold increase in MAN5 ($Hex_5HeXNAc_2$, 20.3 min) was observed (Fig. 2B).

Overall, we observed characteristic glycans for each cell line, in particular bisecting GlcNAcs and Sd^a carrying *N*-glycans were relatively more abundant in the non-cancerous cell line CCD841CoN. Surprisingly, siOGT did not have an impact on the global *N*-Glycans expressed.

3.4 Global *O*-Glycomic survey in OGT-silenced colon cells

To identify and compare the major *O*-glycans in siOGT and siControl cells, PGC-LC-MS/MS was used to analyze reduced *O*-Glycans. Structures were verified using MS/MS fragmentation allowing in most cases to distinguish specific linkages (Table S2). Figure 3A shows the EIC profiles of the major *O*-glycans in the three cell lines. Several structures were common among the three cell lines: $Hex_1HexNAc_1NeuAc$ (sialyl-T-antigen), $Hex_1HexNAc_1NeuAc_2$ (disialyl-T-antigen), monosialylated core 2 $Hex_2HexNAc_2NeuAc_1$ and the disialylated core2 $Hex_2HexNAc_2NeuAc_2$, which is the most abundant *O*-glycan recorded. Interestingly, in agreement with the suppression of core 4 structures in CRC [4], we identified an extended core 4 structure, $Hex_2HexNAc_2NeuAc_2$, only in CCD841CoN cells (Fig. 3A). Quantification showed a slight increase of sialyl-T-antigen and disialyl-T-antigen in siOGT HT29 cells (Fig. 3B). Interestingly, the most abundant glycan $Hex_2HexNAc_2NeuAc_2$, a core 2 structure which has two α2,3-sialic acids linked to galactose decreased significantly in both siOGT HT29 and siOGT CCD841CoN cells. Overall, *O*-glycosylation analyses revealed both similarities and discrepancies among the three cell lines. As observed for *N*-glycans, no dramatic modifications in *O*-Glycan profiles

were observed following OGT silencing.

3.5 Effect of OGT silencing on GSLs expression in HCT116 cells

GSLs from siControl and siOGT transfected cells were analyzed by MALDI-QIT-TOF MS. Representative GSLs acquired in the *m/z* region 1000-1900 are shown in Figure 4. These analyses revealed the presence of three GSLs series namely lactosylceramide (LacCer), globosides (Gb) and gangliosides (Gg). The ceramide moiety (Cer) of the main identified GSLs contained either palmitic acid C16:0 or lignoceric acid C24:0 associated to C18:1 sphingosine (Table S3). Numerous differences in GSLs composition were observed between the three cell lines (Fig. 4). Compared with CCD841CoN cells, the two colon cancer cell lines displayed a high level of LacCer, consistent with the increase of the Lactosyl-Cer synthase (β4GalT-V) expression and activity in CCR tissues [26]. The relative intensity of Gb3 was higher in HCT116 cells than in CCD841CoN and HT29 cells, in agreement with a previous work showing that Gb3 is up-regulated in metastatic colon cancer cells and is important for invasiveness properties of cancer cells [27]. In contrast, GM3 ganglioside accounted for more than 70% of the GSLs in CCD841CoN while it accounted only for 5% of GSLs in HCT116 and was nearly undetectable in HT29 cells. Interestingly, GM3 is likely to be a negative regulator of cancer cell proliferation and mediates cisplatin-induced apoptosis in HCT116 cells [28,29].

When comparing siControl with siOGT cells, LacCer relative abundance decreased by 20% in HT29 while it increased by 30% in HCT116. Similar tendency was observed in CCD841CoN albeit the difference was not statistically significant. In response to siOGT, a significant upregulation by 25-30% of the neutral globoside GSLs was observed in the CRC cell lines, while similar tendency was observed in CCD841CoN cells (Fig. 4B). The relative intensity of Gb3 was increased in the three cell lines and Gb4 increased in HCT116 only (Fig. 4A) [30]. In contrast, the proportion of gangliosides decreased in CCD841CoN and HCT116 cells (Fig. 4C). Beyond modifications in the glycan moiety of GSLs following silencing of OGT, we also observed differences in the acyl group for some glycolipids structures (Fig. 4A and Table S3). These experiments show for the first time that OGT may have an impact in GSLs synthesis and that its silencing strongly deregulates the ratio of sialylated versus non-sialylated GSLs in cells. Also, whereas we observed similarities among the three cell lines, silencing of OGT resulted in cell type-dependent GSLs modifications.

3.6 Silencing of OGT affects *N*-glycosylation of E-cadherin in HT29 cells

E-cadherin is a membrane glycoprotein involved in the establishment of adherens junctions that stabilize epithelial cell-to-cell interactions. Downregulation of E-cadherin expression is a marker of epithelial-mesenchymal transition (EMT). We have previously shown that downregulation of *O*-

GlcNAcylation by siOGT reduced adhesion and migration properties in the three cell lines [9]. We then investigated whether silencing of OGT modifies glycosylation of E-cadherin in HT29 cells. HCT116 and CCD841CoN cells were not suitable for this set of experiments since E-cadherin is mutated in HCT116 cells [31] and is nearly undetectable in in CCD841CoN cells (Fig. 5A). By Western-blot, we showed that silencing of OGT strongly decreased *O*-GlcNAc levels and OGT expression in HT29 cells (Fig. 5A). Moreover, the expression of E-cadherin was elevated by 1.5-fold in siOGT compared with control cells (Fig. 5A). Despite the higher expression of E-cadherin, *O*-GlcNAcylation of immunoprecipitated E-cadherin was decreased by 80% in siOGT-HT29 cells (Fig. 5B). This result was expected since *O*-GlcNAcylation levels were strongly reduced in siOGT cells (Fig. 5A). Furthermore, we showed by immunofluorescence confocal imaging that the elevated E-cadherin expression was accompanied by a significant increase of its plasma membrane localization in siOGT cells, particularly at the cell-to-cell contact regions (Fig. 5C). Adhesive properties of E-cadherin are modulated by *N*-glycosylation of its extracellular domain [32]. To establish the level of *N*-glycosylation of E-cadherin in siOGT HT29 cells, we used the L-PHA and AAA lectins which recognize respectively the β-1,6-branching GlcNAc and α-1,6-fucosylation on *N*-glycans. E-cadherin was immunoprecipitated from cell lysates and its glycosylation was detected using lectin blotting. Albeit a significant higher expression of E-cadherin in siOGT HT29, this showed that both β1,6-branching GlcNAc and core fucosylation of the protein was decreased by more than 50 % upon siOGT transfection (Fig. 5D). Together, these results show that in siOGT HT29 cells, expression of E-cadherin is increased and its recruitment to the cell surface particularly at cell-to-cell junctions is enhanced. Furthermore, we show that silencing OGT strongly alters both the *O*-GlcNAcylation and *N*-glycosylation levels of E-cadherin.

4. Discussion

O-GlcNAcylation governs numerous cellular processes [1] and downregulation of OGT reduces proliferation, migration, adhesion and metastatic capabilities of cancer cells [7-9, 33]. Complex glycans have been also implicated in cell properties that enhance cancer progression [34] but little evidence linking them to *O*-GlcNAcylation has been reported. We therefore used OMICS platforms, combined with fluorescence imaging and protein biochemistry to tackle the putative regulation of complex glycan biosynthesis by *O*-GlcNAcylation in three distinct colon cell lines.

We first examined the influence of OGT silencing on the expression of genes encoding some GTs and GHs involved in glycans synthesis. Of the 86 genes examined, only 10 were significantly affected by OGT silencing across the three cell lines. Regarding *N*-glycans in siOGT-CCD841CoN cells, we noticed

a down-regulation of MGAT5B encoding a β1,6-N-acetylglucosaminyltransferase involved in GlcNAc-branching on mannose arms and FUT8 responsible for core fucosylation. However, these transcriptomic changes were not correlated with a decrease of the final glycan products, as ascertained by *N*-glycomics and FACS analyses (Fig. 1-2). The lack of correlation between mRNA level, protein expression and enzyme activity is often encountered. This apparent inconsistency may arise from differences between the lifetimes of transcripts and their corresponding proteins. Changes in their respective expression level may thus not overlap during the experimental time course. Conversely, analysis of L-PHA labeling by FACS and confocal microscopy indicates that the branching level of β1,6-GlcNAc increases in a slight but significant manner on siOGT-treated HCT116 and HT29 cell surface but not in the non-cancerous CCD841CoN cells (Fig. 1 and Fig. 5C), whereas silencing of OGT does not affect mRNA levels of MGAT5 (Fig. S1).

It is likely that these changes in cancer cell surface β1,6-GlcNAc branching reflects perturbations in HBP flux [14, 35] or trafficking. Indeed OGT silencing interferes with intracellular protein transport as recently reported for coatomer COP (coat protein) I and COP II protein trafficking pathways [36,37]. OGT silencing might impair vesicular trafficking, thus disrupting the glycosylation machinery and the turnover of GTs and GHs. This may partly explain why changes in GTs or GHs mRNA levels have low consequences on *N*- and *O*-glycosylation patterns.

We were greatly intrigued by the unique cell surface glycosylation pattern expressed by siOGT-HT29 cells. Using confocal imaging and flow cytometry, we noted an increase of the β1,6-GlcNAc branching and a global decrease of the core-fucosylated *N*-glycans labeling (Fig. 1 and 5C). Intriguingly, both L-PHA and AAA labeling merged with most of the E-cadherin labeling at cell-cell junctions in HT29 cells (Fig. 5C). We ascertained E-cadherin glycosylation by immunoprecipitation and showed for the first time that both β1,6-GlcNAc branching and core-fucosylation strongly decreased upon OGT silencing (Fig. 5D), independently of a transcriptional regulation of the respective GTs MGAT5 and FUT8 (Fig. S1). We conclude that the overall cell surface glycosylation does not necessarily reflect the glycosylation of individual proteins, as we show here for the L-PHA staining that globally increased at the cell surface but decreased on E-cadherin. The effect of α1,6-fucosylation of E-cadherin is likely to be cellular model-dependent and may impact E-cadherin turnover and β-catenin nuclear level [32]. The increase of β1,6-GlcNAc branching structures on E-cadherin is usually associated with malignancy and loss of its adhesive properties. Conversely, knockdown of MGAT5 reduces *N*-glycosylation of E-cadherin, concomitantly to an increase of its cell membrane localization and interaction with β-catenin [32, 38, 39]. These observations taken together may partly explain the decrease in migration properties that we previously reported in siOGT-HT29 cells [9]. Moreover, OGT silencing increases E-cadherin expression (Fig. 5A). It may be linked with downregulation of the E-cadherin transcriptional

repressor Snail1 which is stabilized by *O*-GlcNAcylation [40]. Accordingly, siOGT may affect Snail1 repression leading to E-cadherin accumulation. Besides its *N*-glycosylation, we showed that *O*-GlcNAcylation of E-cadherin was reduced following OGT silencing (Fig. 5B). *O*-GlcNAcylation of E-cadherin could affect its *N*-glycosylation pattern through a disruption of intracellular trafficking. Indeed, *O*-GlcNAcylation of E-cadherin has been shown to inhibit its export from the endoplasmic *reticulum* [41]. It is likely that silencing of OGT reverses the EMT in HT29 cells through up-regulation of E-cadherin expression and a decrease of β1,6-GlcNAc branching *N*-glycans.

Concerning *O*-linked glycans, although we did not observe major changes in global *O*-glycan profiles (Fig. 3), we reported a downregulation of the mucin-type core 2 synthase GCNT3 whose expression depends on CRC stage [42], and the polypeptide GALNT (*N*-acetylgalactosaminyltransferases)-6, 8, 10 and 16. GALNTs are more active in CRC [43] and responsible for initiating mucin-type *O*-Glycan synthesis, the initial product being the Tn-antigen (Ser/Thr-αGalNAc) [43]. Interestingly, GALNT6 transcripts are upregulated in colon adenocarcinoma, correlated with a cancer-like dysplastic growth [44]. GALNT6 knock-down results in increased cell-cell adhesion and a more differentiated phenotype [44]. In addition, GALNT6 transcription is induced by over activation of HBP in A549 pulmonary cancer cells cultured in hyperglycemic conditions [45]. Taken together, these data suggest that the transcription of GALNT6, a critical and early oncogenic player, is regulated through the HBP/*O*-GlcNAc axis in colon cells. Truncated mucin-type *O*-glycans T (Ser/Thr-αGalNAc[β1-3]Gal) and sTn (Ser/Thr-αGalNAc[α2-6]NeuAc) antigens are a recurring feature in CRC [4]. One of the shortcomings of this study was we were unable to verify a corresponding decrease of truncated *O*-glycans by glycomics as these short forms were not retained on the PGC column. Nonetheless, we observed a slight but significant increase in the sialyl-core 1 glycan (H1N1S1) and disialyl-T-antigen (H1N1S2) in siOGT-transfected HT29 cells and a decrease in the most abundant *O*-glycan $Hex_2HexNAc_2NeuAc_2$ in HT29 and CCD841CoN cells (Fig. 3B), indicating that OGT partly governs *O*-glycan biosynthesis.

The most prominent changes upon silencing of OGT were observed in GSLs. GSLs are a subclass of glycolipids found on the outer side of the cell membrane and play critical roles including plasma membrane stability, adhesion, cell-cell interactions and modulation of signal transduction pathways 30]. Here, GSLs glycomic study revealed that GSL patterns of the three cell lines were modified when OGT expression was silenced (Fig. 4). Of note, the acyl moiety of GM2 was shortened in HCT116 cells following OGT silencing (Fig. 4A). This may arise from a regulation of fatty acid synthase expression and catalytic activity by OGT as previously demonstrated in HepG2 cells [46]. The expression of gangliosides including GM2, GM1 and GD1a, was dramatically decreased in siOGT-transfected HCT116 cells. Surprisingly, GM3, the major precursor of GM1, GM2 and GD1a, was relatively unaffected by siOGT treatment. On the other hand, we found the globo-series glycans Gb3 for the

three cell lines, and Gb4 only in HCT116 cells, to be under the control of *O*-GlcNAcylation, as they were upregulated in siOGT-transfected cells. Overall, we established that OGT-silencing altered the sialylated/non-sialylated GSLs ratio, with upregulation of neutral GSLs and downregulation of sialylated GSLs. These results are in agreement with the suppression of globo-series GSLs during cancer progression [47]. But, carcinogenesis is also associated to an increased-expression and activity of OGT which correlates with enhanced proliferation, migration, invasion, and metastasis [7-9]. To our knowledge this is the very first study linking OGT expression to GSLs remodeling. Surprisingly, following OGT silencing, transcriptomic analysis did not show significant modification in the expression levels of genes encoding enzymes involved in GSLs biosynthesis. The dramatic changes in GSLs composition consecutive to siOGT may originate from a modification of the trafficking or localization of biosynthetic enzymes rather than from modification of their expression levels. Vesicular trafficking is managed by many components among which the COP I and COP II complexes are pivotal, as discussed above [36,37]. Recently, it has been shown that the multiprotein coatomer COP I and COP II are regulated by *O*-GlcNAcylation [36,37]. A perturbation in *O*-GlcNAc homeostasis should affect vesicular trafficking and accordingly complex glycosylation patterns, in particular GSLs that exhibit highly dynamic conformations and adaptability. Nevertheless, the reason why siOGT results in an increases globosides at the expense of gangliosides remain unknown and needs further investigation.

5. Concluding remarks

Herein, we focused on the impact of OGT silencing on the structural changes of complex glycans, particularly *N*- and *O*-glycans, as well as GSLs in various non-pathogenic or cancerous colon cell lines. The first conclusion to be drawn is that we did not observe consistency across the cell lines used, each cell line responding uniquely to OGT silencing. Transcriptomics surprised us not only because very few genes coding GTs and GHs were significantly deregulated, but also because globally we could not observe experimentally significant consequences of the down-regulation of those which were affected. Nonetheless, we observed that siOGT increases the expression of E-cadherin, in agreement with Park and collaborators [40], and also showed it affects its *N*-glycosylation. It would be interesting to measure the effect of the modulation of the expression pattern of the complex glycosylation of E-cadherin on the proliferative, adhesiveness and migratory properties of epithelial cells. The other striking effect of this work is the imbalance caused by siOGT on the sialylated/non-sialylated GSLs ratio, the role of gangliosides in the cancerization process having been well documented. Thus, widely reported disturbances of *O*-GlcNAcylation homeostasis for cancer cells

could impact cell-cell interactions as well as signal transduction by altering this sialylated/non-sialylated GSLs balance. Finally, since it seems that *O*-GlcNAcylation only slightly affects the expression of the enzymes involved in complex glycosylation profiles in particular GSLs, it would be interesting to analyze the intracellular traffic of these major players.

6. Acknowledgements

The authors thank the University of Lille, FRABio FR 3688, the "Centre National de la Recherche Scientifique (CNRS)" and PAGés (http://plateforme-pages.univ-lille1.fr) for their support. J.B. and K.M. are recipients of Marie Curie Innovative Training Network (ITN) fellowships, H2020-EU.1.3.1 (Project ID: 676421, acronym GlyCoCan). We are grateful to Dr Agata Steenackers for the technical assistance and to Dr Sophie Groux-Degroote and Dr. Anne Harduin-Lepers for providing the anti-Sd[a] antibody and helpful discussion. We thank Dr. Corentin Spriet (TISBio core facility) for helping in quantification using ImageJ.

7. Conflict of interest statement

The authors have declared no conflict of interest.

8. References

[1] X. Yang, K. Qian, *Nat Rev Mol. Cell. Biol.* **2017,** 18, 452.
[2] H.J. Gabius, *Biosystems* **2017,** 164, 102.
[3] R.L. Schnaar, A. Suzuki, P. Stanley, in *Essentials of Glycobiology*, 2nd edition. (Eds: A. Varki, R.D. Cummings, J.D. Esko, H.H. Freeze, P. Stanley, C.R. Bertozzi, G.W. Hart, M.E. Etzler), Cold Spring Harbor (NY), Cold Spring Harbor Laboratory Press, **2009,** Ch. 10.
[4] S. Holst, M. Wuhrer, Y. Rombouts, *Adv. Cancer Res.* **2015,** 126, 203.
[5] N. Very, T. Lefebvre, I. El Yazidi-Belkoura, *Oncotarget* **2017,** 9, 1380.
[6] H.B. Ruan, Y. Nie, X. Yang, *Mol Cell Proteomics* **2013,** 12, 3489.
[7] W. Mi, Y. Gu, C. Han, H. Liu, Q. Fan, X. Zhang, Q. Cong, W. Yu, *Biochim. Biophys. Acta.* **2011,** 1812, 514.
[8] T.P. Lynch, C.M. Ferrer, S.R. Jackson, K.S. Shahriari, K. Vosseller, M.J. Reginato, *J. Biol. Chem.* **2012,** 287, 11070.
[9] A. Steenackers, S. Olivier-Van Stichelen, S.F. Baldini, V. Dehennaut, R.A. Toillon, X. Le Bourhis, I. El Yazidi-Belkoura, T. Lefebvre, *Front. Endocrinol.* (Lausanne) **2016,** 7, 46.
[10] C. Phoomak, A. Silsirivanit, D. Park, K. Sawanyawisuth, K. Vaeteewoottacharn, C. Wongkham, E.W. Lam, C. Pairojkul, C.B. Lebrilla, S. Wongkham, *Oncogene* **2018,** 37, 5648.
[11] P. Vella, A. Scelfo, S. Jammula, F. Chiacchiera, K. Williams, A. Cuomo, A. Roberto, J. Christensen, T. Bonaldi, K. Helin, D. Pasini, *Mol. Cell* **2013,** 49, 645.

[12] A. Vasconcelos-Dos-Santos, H.F. Loponte, N.R Mantuano, I.A. Oliveira, I.F. de Paula, L.K. Teixeira, J.C. de-Freitas-Junior, K.C. Gondim, N. Heise, R. Mohana-Borges, J.A. Morgado-Díaz, W.B. Dias, A.R. Todeschini, *Oncogenesis* **2017,** 6, e306.

[13] S.K. Ghosh, M.R. Bond, D.C. Love, G.G. Ashwell, M.W. Krause, J.A. Hanover, *Front. Endocrinol.* (Lausanne) **2014,** 5, 197.

[14] M.C. Ryczko, J. Pawling, R. Chen, A.M. Abdel Rahman, K. Yau, J.K. Copeland, C. Zhang, A. Surendra, D.S. Guttman, D. Figeys, J.W. Dennis, *Sci. Rep.* **2016,** 6, 23043.

[15] J. Biwi, C. Biot, Y. Guerardel, A.-S. Vercoutter-Edouart, T. Lefebvre, *Molecules,* **2018,** 23, E2858.

[16] L. Masclef, V. Dehennaut, M. Mortuaire, C. Schulz, M. Leturcq, T. Lefebvre, A.-S. Vercoutter-Edouart, *Front. Endocrinol.* **2019,** 10, 106.

[17] S. Groux-Degroote, C. Wavelet, M.-A. Krzewinski-Recchi, L. Portier, M. Mortuaire, A. Mihalache, M. Trinchera, P. Delannoy, N. Malagolini, M. Chiricolo, F. Dall'Olio, A. Harduin-Lepers, *Int. J. Biochem. Cell Biol.* **2014,** 53, 442.

[18] A. Blanas, L.A.M. Cornelissen, M. Kotsias, J.C. van der Horst, H.J. van de Vrugt, H. Kalay, D.I.R. Spencer, R.P. Kozak, S.J. van Vliet, *Glycobiology* **2019,** 29, 137.

[19] Kozak, R. P., Tortosa, C. B., Fernandes, D. L., Spencer, D. I. R., *Anal. Biochem*. **2015,** 486, 38.

[20] B.C. Jansen, L. Hafkenscheid, A. Bondt, R.A. Gardner, J.L. Hendel, M. Wuhrer, D.I.R. Spencer, *PLoS One* **2018**, *13*, e0200280.

[21] P.H. Jensen, N.G. Karlsson, D. Kolarich, N.H. Packer, *Nat. Protoc.* **2012,** 7, 1299.

[22] S. Holst, A.J.M. Deuss, G.W. van Pelt, S.J. van Vliet, J.J. Garcia-Vallejo, C.A.M. Koeleman, A.M. Deelder, W.E. Mesker, R.A. Tollenaar, Y. Rombouts, M. Wuhrer, *Mol. Cell. Proteomics* **2016,** 15, 124.

[23] I. Ciucanu, F. Kerek, *Carbohydr. Res.* **1984,** 131, 209.

[24] C.P. Delannoy, Y. Rombouts, S. Groux-Degroote, S. Holst, B. Coddeville, A. Harduin-Lepers, M. Wuhrer, E. Elass-Rochard, Y. Guerardel, *J. Proteome Res.* **2017,** 16, 156.

[25] N. Yamakawa, J. Vanbeselaere, L.-Y.Chang, S.-Y Yu, L. Ducrocq, A. Harduin-Lepers, J. Kurata, K.F. Aoki-Kinoshita, C. Sato, K.-H. Khoo, K. Kitajima, Y. Guerardel, *Nat. Commun.* **2018,** 9, 4647.

[26] S.B. Chatterjee, J. Hou, V.V.R. Bandaru, M.K. Pezhouh, A.A. Syed Rifat Mannan, R. Sharma, *Biochem Biophys Res Commun.* **2019,** 508, 380.

[27] O. Kovbasnjuk, R. Mourtazina, B. Baibakov, T. Wang, C. Elowsky, M.A. Choti, A. Kane, M. Donowitz, *Proc Natl Acad Sci U S A.*. **2005,** 102, 19087.

[28] T.W. Chung, H.J. Choi, S.J. Kim, C.H. Kwak, K.H. Song, U.H. Jin, Y.C. Chang, H.W. Chang, Y.C. Lee, K.T. Ha, C.H. Kim, *PLoS One.* **2014,** 9, e92786.

[29] D. Zhang, X. Li, F. Guan, *Front. Physiol.* **2018,** 9, 466.

[30] S. Groux-Degroote, M. Rodríguez-Walker, J.H. Dewald, J.L. Daniotti, P. Delannoy, *Prog. Mol. Biol. Transl. Sci.* **2018,** 156, 197.

[31] J.A. **Efstathiou, D.** Liu, J.M. Wheeler, H.C. Kim, N.E. Beck, M. Ilyas, A.J. Karayiannakis, N.J. Mortensen, W. Kmiot, R.J. Playford, M. Pignatelli, W.F. Bodmer. *Proc Natl Acad Sci U S A.* **1999,** 96, 231.

[32] S.S. Pinho, R. Seruca, F. Gärtner, Y. Yamaguchi, J. Gu, N. Taniguchi, C.A. Reis, *Cell. Mol. Life Sci.* **2011,** 68, 1011.

[33] Z. Xu, T. Isaji, T. Fukuda, Y. Wang, J. Gu, J., *J. Biol. Chem.* **2019,** 294, 3117.

[34] S.S. Pinho, C.A. Reis, *Nat. Rev. Cancer* **2015,** 15, 540.

[35] K.S. Lau, E.A. Partridge, A. Grigorian, C.I. Silvescu, V.N. Reinhold, M. Demetriou, J.W. Dennis, *Cell* **2007,** 129, 123.

[36] N.J. Cox, P.M. Luo, T.J. Smith, B.J. Bisnett, E.J. Soderblom, M. Boyce, *Front Endocrinol.* **2018,** 9, 606.

[37] N.J. Cox, G. Unlu, B.J. Bisnett, T.R. Meister, B.M. Condon, P.M. Luo, T.J. Smith, M. Hanna, A. Chhetri, E.J. Soderblom, A. Audhya, E.W. Knapik, M. Boyce M, *Biochemistry* **2018,**;57, 91.

[38] M.K. Hall, D.A. Weidner, S. Dayal, R.A. Schwalbe, *FEBS Open Bio.* **2014,** 4, 892.

[39] H.-B. Guo, I. Lee, M. Kamar, M. Pierce, *J Biol Chem.* **2003, 278**, 52412.

[40] S.Y. Park, H.S. Kim, N.H. Kim, S. Ji, S.Y. Cha, J.G. Kang, I. Ota, K. Shimada, N. Konishi, H.W. Nam, S.W. Hong, W.H. Yang, J. Roth, J.I. Yook, J.W. Cho, *EMBO J.* **2010,** 29, 3787.

[41] F. Geng, W. Zhu, R.A. Anderson, B. Leber, D.W. Andrews, *J. Cell. Sci*. **2012,** 125, 2615.

[42] L.P. Fernández, R. Sánchez-Martínez, T. Vargas, J. Herranz, R. Martín-Hernández, M. Mendiola, D. Hardisson, G. Reglero, J. Feliu, A. Redondo, A. Ramírez de Molina, *Sci. Rep.* **2018,** 8, 8485.

[43] I. Brockhausen, *EMBO Rep*. **2006,** 7, 599.

[44] K. Lavrsen, S. Dabelsteen, S.Y. Vakhrushev, A.M.R. Levann, A.D. Haue, A. Dylander, U. Mandel, L. Hansen, M. Frödin, E.P. Bennett, H.H. Wandall, *J. Biol. Chem*. **2018,** 293, 1298.

[45] F. **Alisson-Silva**, L. Freire-de-Lima, J.L. Donadio, M.C. Lucena, L. Penha, J.N. Sá-Diniz, W.B. Dias, A.R. Todeschini, *PLoS One*. **2013,** 8, e60471.

[46] S.F. **Baldini**, C. Wavelet, I. Hainault, C. Guinez, T. Lefebvre, *J Mol Biol.* **2016,** 428, 3295.

[46] S. Holst, K. Stavenhagen, C.I. Balog, C.A. Koeleman, L.M. McDonnell, O.A. Mayboroda, A. Verhoeven, W.E. Mesker, R.A. Tollenaar, A.M. Deelder, M. Wuhrer, *Mol. Cell. Proteomics* **2013,** 12, 3081.

9. Figure Captions

Figure 1: FACS analysis using lectins shows that OGT silencing differentially affects cell surface glycosylation in HT29, HCT116 and CCD841CoN cells. Unstained siControl cells used as negative control are indicated by a grey line (siControl, neg). Representative fluorescence histograms show the variation in mean of fluorescence for each lectin labeling. The bar graphs indicate the mean +S.D. of the relative fluorescence observed in siOGT-treated cells compared to siControl cells (n≥3). Statistical analysis was performed by Student's *t*-test (*n.s.*, non-significant; * p<0.05, ** p<0.01, ***p<0.005).

Figure 2: Global *N*-glycomic analysis of the effect of siOGT in colon cell lines. Released and procainamide-labelled *N*-glycans were analysed in positive mode on a HILIC-(U)HPLC-ESI-MS system with UV detection. A) Assignments of main glycan peaks detected for each cell line in siCtrl (blue line) and siOGT (orange line) cells. B) The bars show the mean + S.D. of normalized UV intensity for each glycan over 2 biological and 3 technical replicates (** p<0.01).

Figure 3: Global *O*-glycomic analysis of the effect of siOGT in colon cell lines. Released and reduced *O*-glycans were analysed in negative mode by PGC-LC-MS/MS. A) EIC assignments of glycan peaks of interest detected for each cell line in siCtrl (blue line) and siOGT (orange line) conditions. B) The bars show the mean + S.D. of normalized EIC AUC of each glycan over 4 biological replicates. For comparison of glycan abundances between siCtrl and siOGT conditions, AUCs of each glycan structure were normalized to the total AUC (for all glycan structures in a sample summed) and expressed as a percentage. Statistical analysis was performed using *t*-test (* p < 0.05).

Figure 4: Global GSL analysis of the effect of siOGT in colon cell lines. A) MALDI-QIT-TOF-MS profiles of permethylated GSLs in siCtrl and siOGT transfected cells. GSLs are present as d18:1/C16:0, d18:1/C16:1, d18:1/C24:0, and d18:1/C24:1 (see Table S3 for details). B) Structural class pooling of LacCer, globoside and ganglioside series and comparison of their relative intensity between siCtrl and siOGT conditions for each cell line. The bars demonstrate the mean +S.D. of the normalized abundance for each glycan over 3 biological replicates. Statistical analysis was performed using *t*-test (* p < 0.05; ** p < 0.01).

Figure 5: Analysis of E-cadherin expression and glycosylation in siOGT-treated cells. A) Western blot analysis for *O*-GlcNAcylated proteins, OGT, and E-cadherin contents in the three colon cell lines. The bar graph shows the relative level of E-cadherin; tubulin is used as a loading control (means + S.D.; n=3). B) *O*-GlcNAc staining of immunoprecipitated E-cadherin in HT29 cells. The bar graph shows the

relative intensity of the *O*-GlcNAcylated E-cadherin normalized to the total amount of immunoprecipitated E-cadherin (mean + S.D.; n=2). C) Confocal microscopy images of cell surface E-cadherin, L-PHA and AAA binding in siOGT compared to siCtrl HT29 cells (scale bar=20 µm). On the last row, a magnification of the merge images is shown (scale bar=10 µm). Quantification of fluorescence is presented as scatter dot plots; each dot represents the mean of fluorescence of a single cell. Bars represent the median with interquartile range for both experimental conditions. D) E-cadherin was immunoprecipitated in HT29 cell lysates and membranes were probed first with L-PHA-biotin or AAA-FITC (upper panel). After stripping, membranes were probed with an anti-E-cadherin antibody (lower panel). The bar graphs show the relative intensity of glycosylated E-cadherin normalized to the amount of total immunoprecipitated E-cadherin (mean + S.D.; n=2). Statistical analyses were performed by *t*-test (** $p<0.05$; *** $p<0.005$).

Supplemental Figures

Figure S1: Transcriptomic analysis of the effect of OGT silencing in colon cell lines. A) Volcano plots of 86 glyco-genes (listed in Table S1) of siOGT versus siCtrl cells. The genes significantly downregulated are indicated by a blue spot. The significance threshold is indicated by a horizontal red line. B) Histogram showing the fold change for OGT and OGA mRNA levels in siOGT versus siCtrl-treated cells for the three cell lines. C) Western-blot showing the down-regulation of *O*-GlcNAcylated proteins, OGT and OGA protein levels in siOGT-transfected cells. GAPDH was used as a loading control. D) Western-blot using the anti-O-GlcNAc antibody (RL2) incubated with or without 0.2M GlcNAc to ascertain the specificity of the antibody. Tubulin was used as a loading control.

Figure S2: Sd^a antigen is down-regulated in siOGT-treated CCD841CoN cells. (A) Detection by Western-blot of Sd^a antigen and OGT in siCtrl- and siOGT-treated- cells. GAPDH was used as a loading control. (B) Bar graph showing the relative intensity of Sd^a antigen in siOGT compared with siCtrl CCD841CoN cells (mean + S.D.; n=4). Statistical analysis was performed by *t*-test (*** $p<0.005$).

Supplemental Tables

Table S1. List of genes used for the transcriptomic analysis. The ΔCt are also reported for each group of the three colon cell lines (3 biological replicates).

Table S2. *N*-glycan and *O*-glycan MS peak lists from the three colon cell lines. Column 1 shows elution or acquisition time, column 2 is the LC-peak identification in glucose procainamide units for *N*-Glycans or shorthand composition for *O*-glycans. Proposed structures predicted from parent peaks and MS/MS fragments (Column 3) and the monosaccharide composition for each glycan (column 4). Predicted and observed masses for each glycan are listed in columns 5-7. Fragment ions used to predict and elucidate structural information are shown in the last columns. (Hexose = Hex, H; *N*-acetylhexosamine = HexNAc, N; N-acetylneuraminic acid = Neu5Ac, S; fucose = Fuc, F; proc = procainamide).

Table S3. The sequence of carbohydrate moieties and the nature of ceramides were established by MS/MS fragmentation of permethylated GSLs in positive mode. *m/z* values correspond to the $[M+Na]^+$ adducts of individual permethylated GSLs. Most probable combinations of sphingoid bases and fatty acids based on *m/z* values of permethylated GSLs are reported in the corresponding columns. C16:0 and Ch16:0 correspond to non-hydroxylated and hydroxylated fatty acids, respectively. Conclusive presence of individual GSLs is reported in the last three columns as ✓. Hexose = Hex; *N*-acetylhexosamine = HexNAc; *N*-acetylneuraminic acid = Neu5Ac; Ceramide = Cer.

FIGURE 1

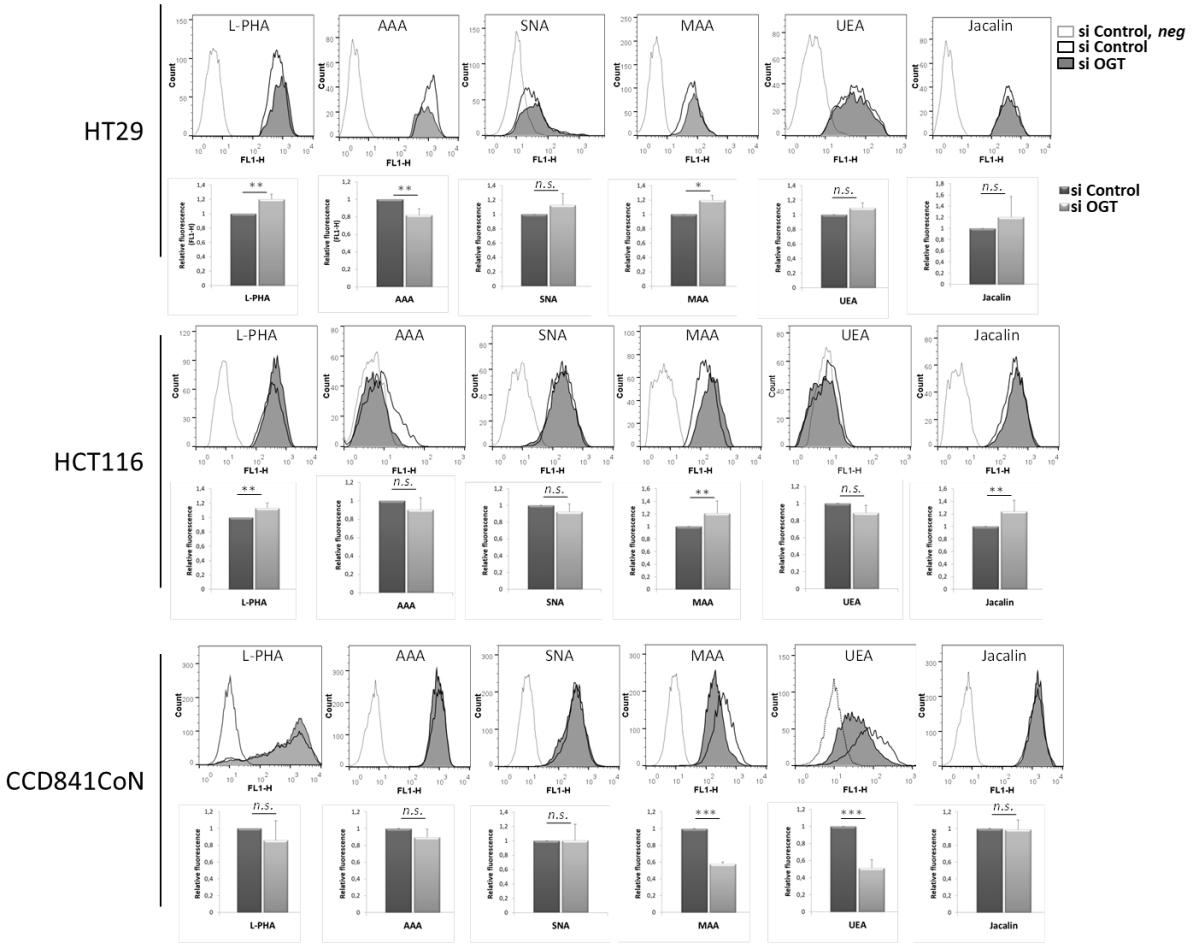
HT29
HCT116
CCD841CoN
L-PHA
AAA
SNA
MAA
UEA
Jacalin
si Control, neg
si Control
si OGT
Count
FL1-H
Relative fluorescence
n.s.

FIGURE 2

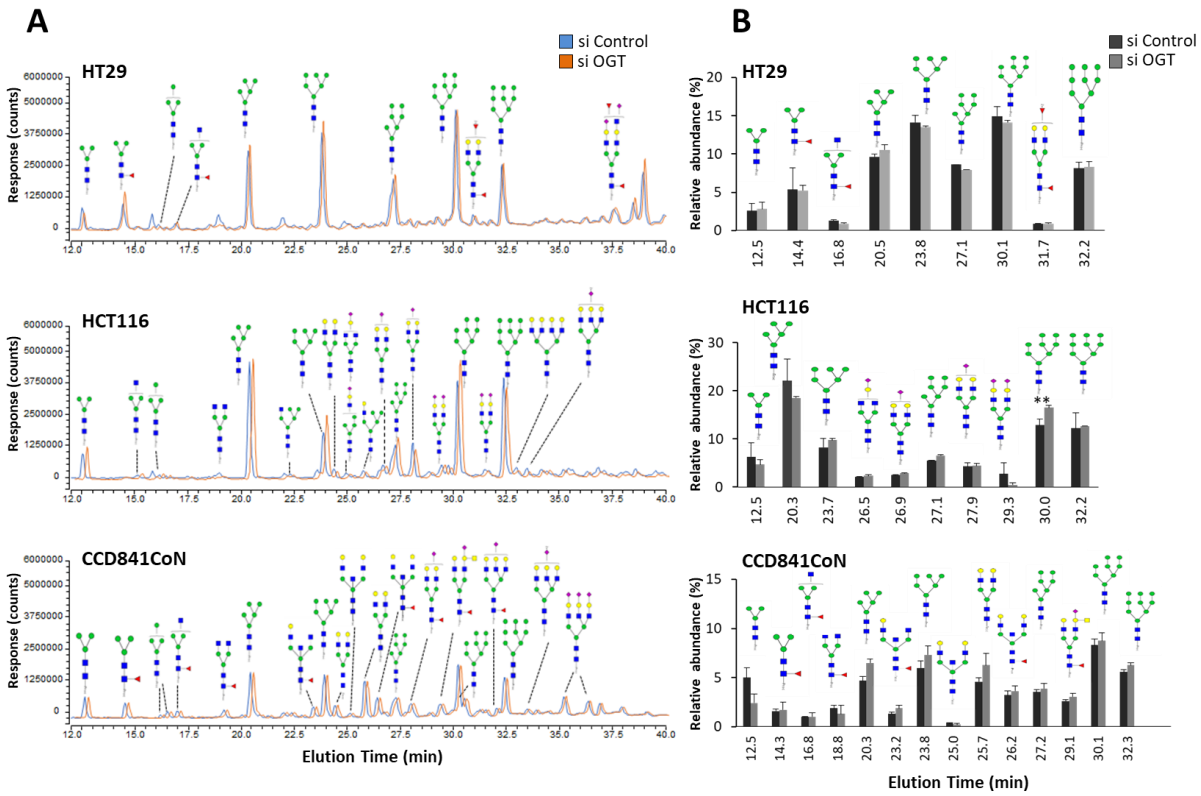
A
B
si Control
si OGT
HT29
HCT116
CCD841CoN
Response (counts)
Relative abundance (%)
Elution Time (min)
**

FIGURE 3

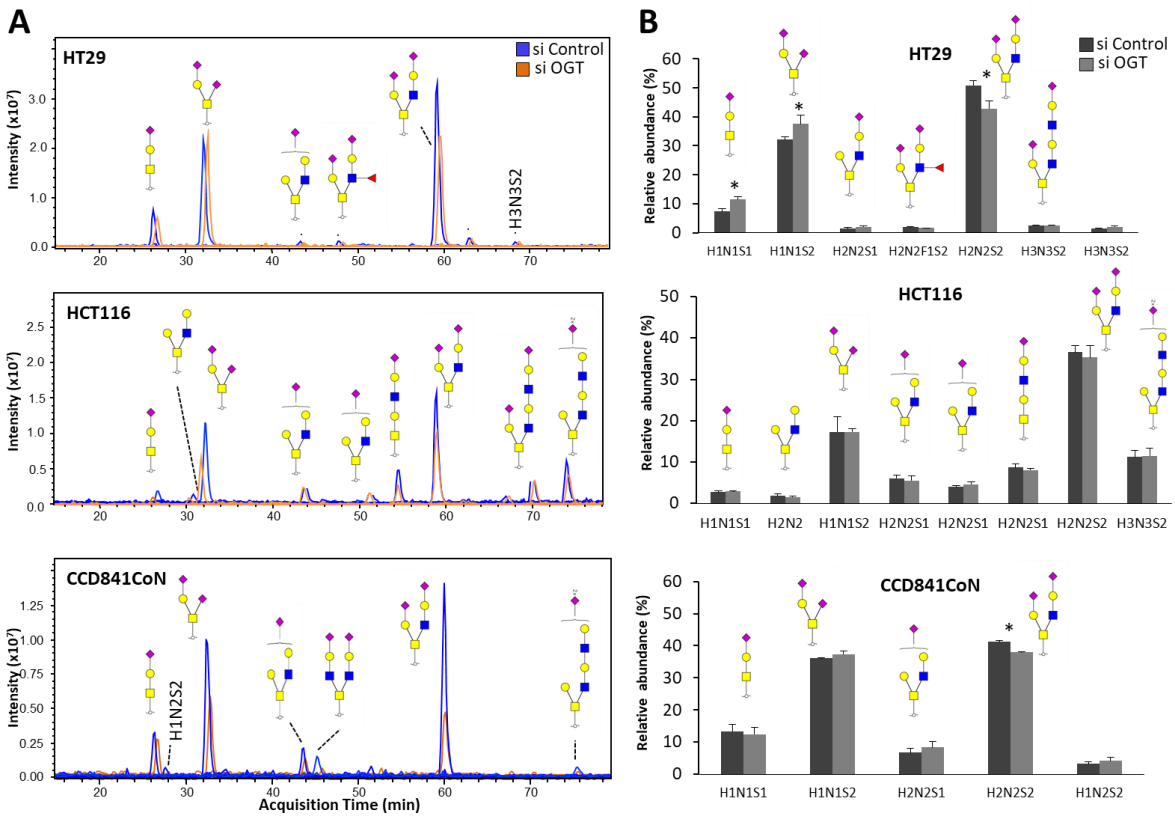
A
HT29
si Control
si OGT
H3N3S2
Intensity (x10⁷)
HCT116
CCD841CoN
H1N2S2
Acquisition Time (min)
B
HT29
si Control
si OGT
Relative abundance (%)
H1N1S1
H1N1S2
H2N2S1
H2N2F1S2
H2N2S2
H3N3S2
HCT116
H2N2
CCD841CoN
H1N2S2

FIGURE 4

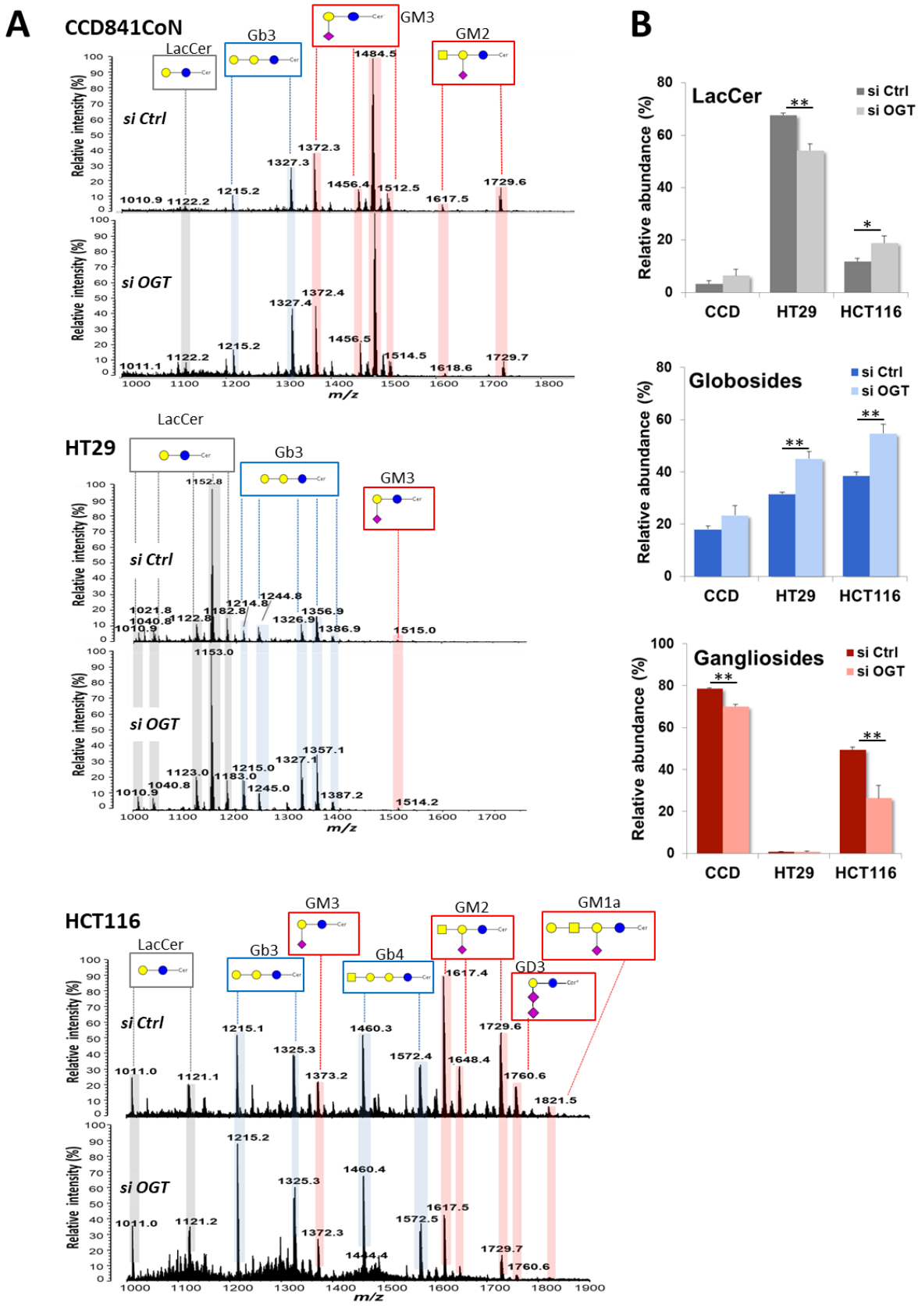
A
CCD841CoN
LacCer
Gb3
GM3
GM2
si Ctrl
si OGT
Relative intensity (%)
m/z
HT29
Gb3
GM3
LacCer
HCT116
Gb3
Gb4
GM3
GM2
GM1a
GD3
B
LacCer
Globosides
Gangliosides
si Ctrl
si OGT
Relative abundance (%)
CCD
HT29
HCT116

FIGURE 5

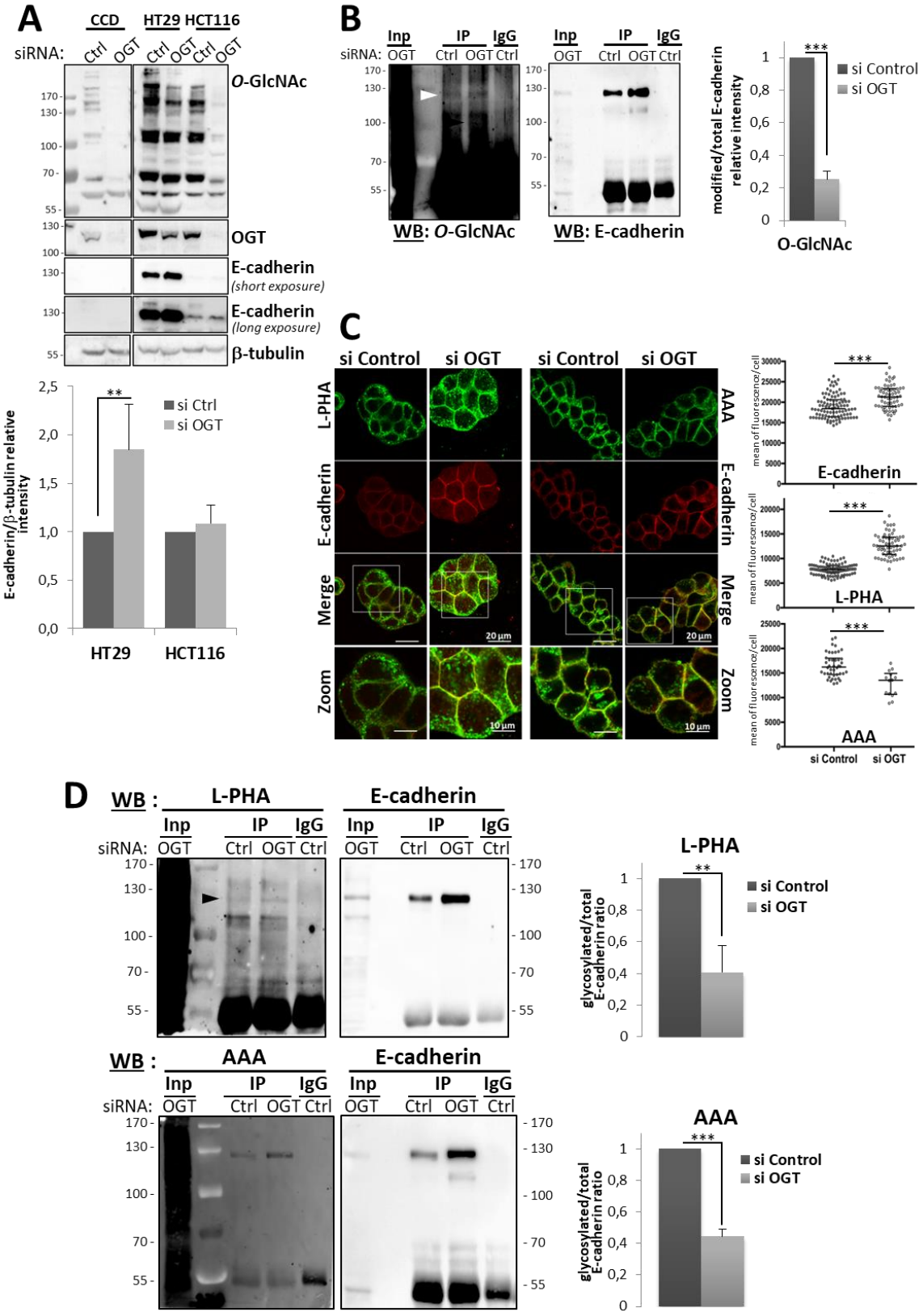
A
CCD
HT29 HCT116
siRNA: Ctrl OGT Ctrl OGT Ctrl OGT
O-GlcNAc
OGT
E-cadherin
(short exposure)
E-cadherin
(long exposure)
β-tubulin
E-cadherin/β-tubulin relative intensity
si Ctrl
si OGT
HT29
HCT116
B
Inp IP IgG
siRNA: OGT Ctrl OGT Ctrl
WB: O-GlcNAc
WB: E-cadherin
modified/total E-cadherin relative intensity
si Control
si OGT
O-GlcNAc
C
si Control
si OGT
L-PHA
E-cadherin
Merge
Zoom
AAA
mean of fluorescence/cell
D
WB : L-PHA
WB : AAA
E-cadherin
glycosylated/total E-cadherin ratio

FIGURE S1

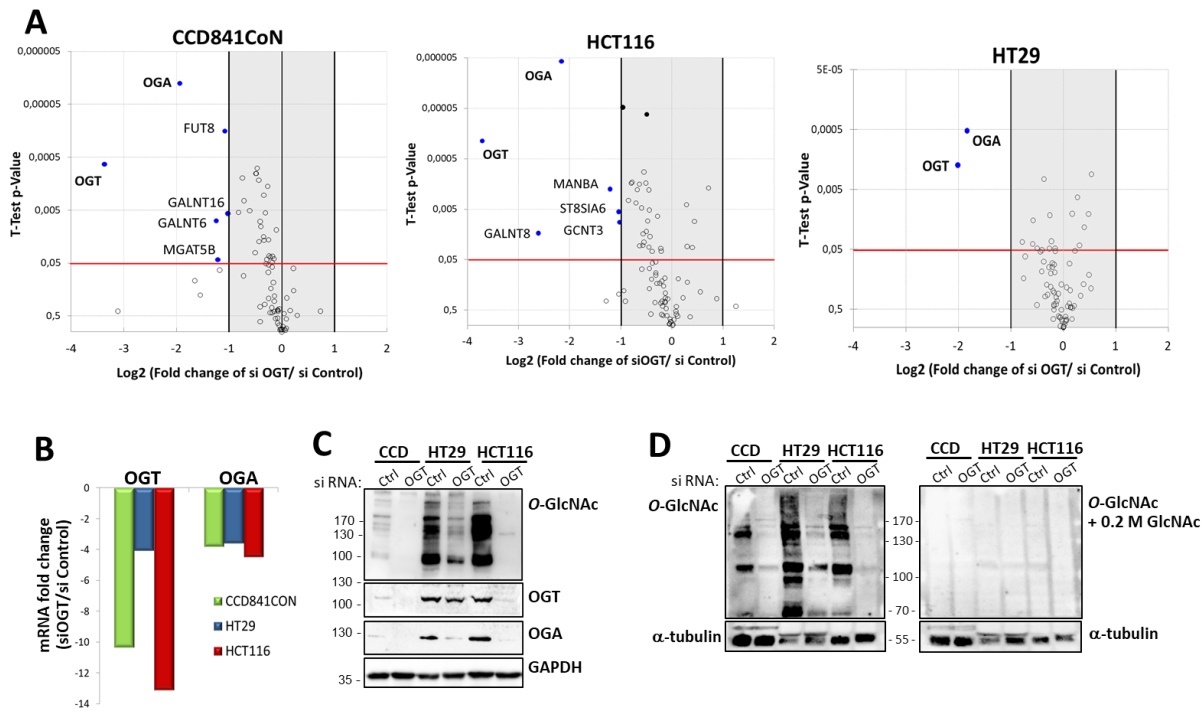
A
CCD841CoN
HCT116
HT29
OGA
OGT
FUT8
GALNT16
GALNT6
MGAT5B
MANBA
ST8SIA6
GCNT3
GALNT8
T-Test p-Value
Log2 (Fold change of si OGT/ si Control)
Log2 (Fold change of siOGT/ si Control)
B
OGT
OGA
mRNA fold change (siOGT/si Control)
CCD841CON
HT29
HCT116
C
CCD HT29 HCT116
si RNA: Ctrl OGT Ctrl OGT Ctrl OGT
O-GlcNAc
OGT
OGA
GAPDH
D
CCD HT29 HCT116
si RNA: Ctrl OGT Ctrl OGT Ctrl OGT
O-GlcNAc
α-tubulin
O-GlcNAc + 0.2 M GlcNAc

TABLE S3

Lacto serie

m/z	Type	Fatty acids	Shingoid base	Composition	CCD	HT29	HCT116
1011.0	LacCer	C16:0	d18:1	Hex2-Cer	✓	✓	✓
1040.8	LacCer	Ch16:0	d18:1	Hex2-Cer		✓	
1121.2	LacCer	C24:1	d18:1	Hex2-Cer	✓	✓	✓
1123.0	LacCer	C24:0	d18:1	Hex2-Cer	✓	✓	✓
1152.8	LacCer	Ch24:0	d18:1	Hex2-Cer		✓	
1182.8	LacCer	C26:0	d18:2	Hex2-Cer		✓	

Globo-serie

m/z	Type	Fatty acids	Shingoid base	Composition	CCD	HT29	HCT116
1215.2	Gb3	C16:0	d18:1	Hex3-Cer	✓	✓	✓
1244.8	Gb3	C18:0	d18:1	Hex3-Cer		✓	
1246.8	Gb3	C16h0	d18:1	Hex3-Cer		✓	
1325.3	Gb3	C24:1	d18:1	Hex3-Cer	✓	✓	✓
1327.3	Gb3	C24:0	d18:1	Hex3-Cer	✓	✓	✓
1329.3	Gb3	Ch22:0	d18:1	Hex3-Cer		✓	
1356.9	Gb3	Ch24:0	d18:1	Hex3-Cer		✓	
1386.9	Gb3	C26:1	d18:1	Hex3-Cer		✓	
1388.9	Gb3	C26:0	d18:1	Hex3-Cer		✓	
1460.3	Gb4	C16:0	d18:1	Hex3HexNAc1-Cer			✓
1572.4	Gb4	C24:0	d18:1	Hex3HexNAc1-Cer			✓

Ganglioside-serie

m/z	Type	Fatty acids	Shingoid base	Composition	CCD	HT29	HCT116
1372.3	GM3	C22:0	d18:1	Neu5Ac1Hex2-Cer	✓		✓
1456.4	GM3	C22:0	d18:1	Neu5Ac1Hex2-Cer	✓		
1484.5	GM3	C24:0	d18:1	Neu5Ac1Hex2-Cer	✓		
1512.5	GM3	C26:0	d18:1	Neu5Ac1Hex2-Cer	✓		
1514.5	GM3	Ch24:0	d18:1	Neu5Ac1Hex2-Cer	✓	✓	
1617.5	GM2	C16:0	d18:1	Neu5Ac1Hex2HexNAc1-Cer	✓		✓
1648.4	GM2	C20:1	d18:1	Neu5Ac1Hex2HexNAc1-Cer			✓
1727.7	GM2	C24:1	d18:1	Neu5Ac1Hex2HexNAc1-Cer	✓		✓
1729.7	GM2	C24:0	d18:1	Neu5Ac1Hex2HexNAc1-Cer	✓		✓
1760.6	GD3	C18:0	d18:1	Neu5Ac2Hex2-Cer			✓
1821.5	GM1a	C16:0	d18:1	Neu5Ac1Hex3HexNAc1-Cer			✓